

Observation Constrained Aromatic Emissions in Shanghai, China

Key Points:

- Differences were found in aromatics characteristics between model simulations and measurements
- Observation-constrained aromatic emissions were estimated in Shanghai
- Aromatic emissions exhibited clear monthly variations

Supporting Information:

- Supporting Information S1

Correspondence to:

H. Wang, R. Yan and Y. Wang,
wanghl@saes.sh.cn;
yanrs@saes.sh.cn;
yuhang.wang@eas.gatech.edu

Citation:

Wang, H., Yan, R., Xu, T., Wang, Y., Wang, Q., Zhang, T., et al. (2020). Observation constrained aromatic emissions in Shanghai, China. *Journal of Geophysical Research: Atmospheres*, 125, e2019JD031815. <https://doi.org/10.1029/2019JD031815>

Received 14 OCT 2019

Accepted 28 FEB 2020

Accepted article online 5 MAR 2020

Hongli Wang¹ , Rasha Yan^{1,4}, Tingting Xu^{2,1}, Yuhang Wang³ , Qian Wang¹, Tianqi Zhang^{1,5}, Jingyu An¹, Cheng Huang¹, Yaqin Gao¹, Yang Gao⁵ , Xiang Li² , Chao Yu⁶, Shengao Jing¹, Liping Qiao¹, Shengrong Lou¹ , Shikang Tao¹, and Yingjie Li¹

¹Shanghai Academy of Environmental Sciences, State Environmental Protection Key Laboratory of Formation and Prevention of Urban Air Pollution Complex, Shanghai, China, ²Shanghai Key Laboratory of Atmospheric Particle Pollution and Prevention (LAP3), Department of Environmental Science and Engineering, Institute of Atmospheric Sciences, Fudan University, Shanghai, China, ³School of Earth and Atmospheric Sciences, Georgia Institute of Technology, Atlanta, GA, USA, ⁴Collaborative Innovation Center of Atmospheric Environment and Equipment Technology, Jiangsu Key Laboratory of Atmospheric Environment Monitoring and Pollution Control, School of Environmental Science and Engineering, Nanjing University of Information Science and Technology, Nanjing, China, ⁵Key Laboratory of Marine Environmental Science and Ecology, Ministry of Education, Ocean University of China, Qingdao, China, ⁶State Key Laboratory of Remote Sensing Science, Institute of Remote Sensing and Digital Earth, Chinese Academy of Sciences, Beijing, China

Abstract Aromatics in the atmosphere are a large contributor to ozone and secondary organic aerosol formation and have an adverse impact on human health. Observation-based emissions are urgently needed for air quality management and decision making due to the large uncertainties in the emissions inventories. Atmospheric aromatics were continuously observed at one urban site in Shanghai of China in 2015, which were compared with the simulations of the Community Multiscale Air Quality (CMAQ) model. Large differences were found in the temporal variations between the model and measurements, corroborating with previous studies that the current bottom-up emission inventories are highly biased. We corrected the aromatic emissions biases of the emission inventories using the observations with the CMAQ simulations, with the assumption that the response relationship of the emissions input and aromatic concentrations was reasonable on a monthly basis in CMAQ simulations, suggesting that the results are dependent on the model performance. The resulting aromatic emissions exhibited clear monthly variations, increasing from 5.5 ± 2.1 Gg month⁻¹ in February to 17.4 ± 7.7 Gg month⁻¹ in July, being different from the flat monthly pattern in the current bottom-up emissions inventory. Toluene, xylenes, and ethylbenzene dominated aromatic emissions, accounting for ~74% on average but with considerable monthly variations, which was different from the nearly uniform value of 77% throughout the whole year in the emissions inventory. These highly temporally resolved and speciated in situ aromatics measurements provide observation-based constraints on aromatic emissions, which cannot be obtained from satellite measurements. This study proposes a top-down emission estimation method constrained by ambient measurements.

1. Introduction

Aromatics hydrocarbons (referred to as aromatics herein) are of great interest in the atmosphere due to their important roles in tropospheric photochemistry (Atkinson, 2000; Cabrera-Perez et al., 2016; Seinfeld & Pandis, 2012). Aromatics have been found to be the largest contributor of ozone formation (or formation potential) either through direct observation or via the calculation of emission inventories in most urban areas in China (Barletta et al., 2005; Kansal, 2009; Lee et al., 2002; Liu et al., 2012; Ran et al., 2009). Meanwhile, aromatics are the most important anthropogenic volatile organic precursors of secondary organic aerosols (SOA) in urban areas in eastern China, which contributed more than 80% of SOA formation from anthropogenic volatile organic compounds (VOCs) (Ding et al., 2012; Guo et al., 2014; Kanakidou et al., 2005; Yuan et al., 2013).

Aromatics are mainly emitted from anthropogenic activities, including combustion processes, solvent usage, vehicular exhausts, and industrial chemical and petrochemical processes (Ceron-Breton et al., 2015; Kumar

et al., 2018; P. Shao et al., 2016; Wang, Chen, et al., 2013). The variety, complexity, and collocation of aromatic sources make it difficult to accurately estimate emissions from individual sources (Fu et al., 2007; Liu et al., 2012; Zhang et al., 2017). The “bottom-up” inventory approach, which involves summing the products of activity data and emissions factors for all known individual sources, results in emission inventories with large uncertainties.

In contrast, “top-down” emission inventories are constrained by observations of relevant data, including ground observations (de Gouw, 2005; Hsu et al., 2010; M. Shao et al., 2011; Wang et al., 2014) and satellite observations (Fu et al., 2007; Liu, Wang, Vrekoussis, et al., 2012; Zhang et al., 2017); “top-down” inventories are increasingly used to validate the bottom-up emission inventories. Using the ground measurements, de Gouw (2005) developed a parameterized method to estimate VOC emissions from carbon monoxide (CO) emission inventories and emission ratio of VOCs to CO, assuming that VOCs and CO were coemitted from the same sources (specifically, from combustion sources). Unfortunately, this assumption was unsuitable for most regions of China, where VOCs were emitted from complex sources, and aromatics in particular arise from a variety of industrial processes (Liu et al., 2019; Wang et al., 2013). Chen et al. (2010) modified the Taiwan Air Quality Model by correcting VOC emission inputs using ratios of observed VOCs and primary model results (Chen et al., 2010).

Satellite observations, which are usually combined with model simulations, are useful for estimating and validating aromatic emissions but suffer from low time and speciated resolution (Fu et al., 2007; Liu, Wang, Vrekoussis, et al., 2012; Zhang et al., 2017).

This study explored a new approach for estimating aromatic emissions by combining ground observations with the Community Multiscale Air Quality (CMAQ) 3-D regional air quality model simulations. Observation-constrained aromatic emissions in Shanghai, China in 2015 were used to validate the monthly variations and specific compositions of the emission inventories available.

2. Materials and Methods

2.1. Monitoring Site

Continuous measurements were performed on the rooftop of a building (~15 m above ground level) in the Shanghai Academy of Environmental Sciences (SAES, 31.17°N, 121.43°E), which is located in an urban area in southwest central Shanghai, China. Vehicular and domestic emissions were the dominant VOC emissions in this area; petrochemical and chemical industrial facilities located 50 km south and southwest of the measurement site may impact the VOC composition observed at the measurement site under specific meteorological conditions (Wang, Chen, et al., 2013). Northwest and southeast winds prevail in this region during the cold and warm seasons, respectively (H. L. Wang et al., 2016); thus, the SAES site, which can be considered a receptor site, is influenced by a wide mixture of emissions and their evolution.

2.2. Measurements

A total of 17 aromatics were observed, including benzene; toluene; ethylbenzene; m-, p-, and o-xylene; styrene; iso- and n-propylbenzene; m-, p-, and o-ethyltoluene; 1,3,5-, 1,2,4-, and 1,2,3-trimethylbenzene; and m- and p-diethylbenzene. These species were measured continuously at 30-min resolution from January to December 2015 using online high-performance gas chromatograph with a flame ionization detector (Chromato-sud airmoVOC C6-C12 #2260308, France). The detection limits of these compounds were between several tens to hundreds of pptv, and the statistics results of the measurements of each species were summarized in Supporting Information Table S1. As shown, more than 75% concentrations of benzene, toluene, ethylbenzene, and xylenes were higher than the detection limit, which were focused on in the present study. Concentrations of the other species were generally lower than the detection limit, of which uncertainties were relatively high as listed in Table S1.

The calibration of the gas chromatograph with a flame ionization detector in this study included two parts. One was the multiple-point calibration with the standard gases (Spectra, United States) each month, and the calibrated concentrations were 0.0, 0.5, 1.0, 2.0, and 4.0 ppbv. The calibration curve was used to recalculate the concentrations of the target species. The other one was the stability validation of the instrument response by the single-point calibration using the standard matter (benzene) in the permeation tube, and the response

of the instrument was stable with the fluctuations with $\pm 10\%$, as shown in Figure S1. Detailed instrument procedures have been described previously (Wang, Chen, et al., 2013).

2.3. CMAQ Model

Because aromatics were measured at only one ground-level site, spatial and vertical distributions of aromatics concentrations were simulated by CMAQ v5.0 (<https://www.cmascenter.org/cmaq/>). The Carbon Bond 05 chemistry, Regional Acid Deposition Model (RADM) aqueous chemistry, AERO5 aerosol, and the SOAP SOA chemistry mechanisms were used in the CMAQ simulations.

Two-way nested domains were adopted in CMAQ herein. The parent domain covering the whole China had a horizontal grid resolution of 36 km and contained 136×196 grid cells in each vertical layer. The nested domain covering the Yangtze River Delta region had a finer scale, with 12-km grid resolution and includes 105×120 grid cells. The D01 and D02 domains were based on a Lambert conformal projection with a reference longitude of 118°E and latitude of 32°N . The 27 vertical layers from Weather Research and Forecasting (WRF) model were mapped onto 14 vertical layers extending from the surface to 100 mb in CMAQ. WRF (Ver 3.7.1; <http://www2.mmm.ucar.edu/wrf/users/>) was run simultaneously for the two nested domains with two-way feedback between the parent and the nest grids. Shanghai domain included 10×10 horizontal grids with grid resolution of 12-km spacing (Figure S2). The CMAQ model has been detailed elsewhere (L. Li et al., 2016; L. Li et al., 2012). The emissions inventory used for the D01 domain was based on the MEIC-2012 anthropogenic inventory for China, which was developed by Tsinghua University (<http://www.meicmodel.org/>) (M. Li et al., 2014). The emissions inventory used for the Yangtze River Delta region was updated in 2014. Biogenic inventories for D01 and D02 were driven by Model of Emissions of Gases and Aerosols from Nature (Liu et al., 2018). The domain settings were provided in Figure S2.

WRF performance for the simulation of hourly surface temperature, relative humidity, and wind speed and direction was evaluated through comparison with observations from the meteorological measurements at Pudong International Airport in Shanghai. Mean bias, gross error, root mean square error, and index of agreement are commonly used for the evaluation of meteorology variables. The ranges of biases, summarized in Table S2, mostly met the model performance criteria recommended by Emery et al. (2001) for retrospective regional-scale model applications that are $\leq \pm 0.5$ K, $\leq \pm 1.0$ g/kg, $\leq \pm 0.5$ m s⁻¹, and $\leq \pm 10^\circ$, respectively, suggesting that the meteorology simulations in this study were acceptable. The evaluation of WRF performance ensured that there was no significant bias in the meteorological fields used in the coupled model.

3. Results and Discussion

3.1. Comparison Between Field Measurements and CMAQ Model Simulations

The annual concentration of aromatics in Shanghai urban was 5.4 ± 1.1 ppbv (mean \pm standard variations of monthly concentrations) on average, taking up 23% of the concentration of nonmethane hydrogen carbons, based on the 1-year measurement at SAES site in 2015. Among them, toluene was the most abundant species, accounting for 34% of total aromatics, followed by m- and p-xylene (19%), ethylbenzene (15%), benzene (14%), and o-xylene (6%), and the other species measured in this study contributed 12% of aromatics together. Aromatic concentrations and compositions had large monthly variations with a “W” mode, and three peaks of concentrations were observed, that is, in January, June, and December, as shown in Figures 1a and 1b. These observed monthly patterns arose from a combination of meteorological conditions, local emissions, and photochemical process in Shanghai, which was discussed previously (Wang, Chen, et al., 2013). Toluene and benzene proportions in total aromatics were lower in summer than those in other seasons, while the monthly C9–C10 aromatic (sign as others in Figure 1) proportions were opposite with those of toluene. It suggested that the relative contribution of combustion emissions, indicated by benzene, increased in cold seasons, while the higher proportions of C9–C10 aromatics in summer suggested more emissions from solvent usage (Wang et al., 2014). The proportions of other species were relatively flat. In terms of the diurnal patterns, as shown in Figure 2, the lowest concentrations presented at 13:00, mainly due to the strongest photochemistry and the highest mixing layer height during noontime, and the relative contribution of benzene, the most inert species among aromatics, increased correspondingly. Toluene

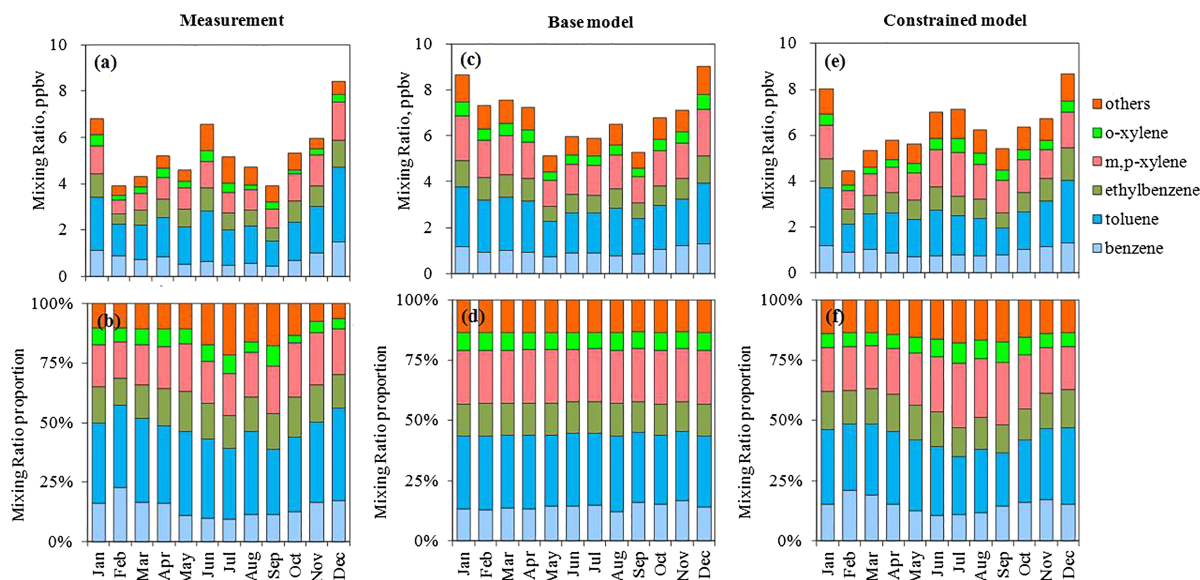


Figure 1. Monthly patterns of aromatic concentrations and speciation from (a, b) in situ observations, (c, d) base CMAQ model simulation, and (e, f) observation-constrained CMAQ model simulation.

concentrations and its relative contributions in the early morning before 8:00 increased significantly, and the increase of traffic emissions might be one important reason.

Monthly variations in aromatics from (Figures 1a and 1b) in situ observations and (Figures 1c and 1d) the base CMAQ model simulation were shown for each month in Figure 1. The yearly average aromatics concentrations of base CMAQ result (6.9 ± 1.2 ppbv, mean \pm standard variations of monthly concentrations) were higher than that of the observed result above. In terms of the monthly variations, the base CMAQ results presented a “U” mode, being different from the “W” mode of observations above. Specifically, base CMAQ failed to reproduce the observed June aromatics peak although CMAQ reproduced the January and December peaks (Figure 1). As to the speciation, the proportions of toluene and ethylbenzene were higher in observed result than those in model result, and benzene’s was close, which were opposite for other species, as shown in Figure 3.

The base model-measurement deviations suggested large uncertainties in the aromatic emission inventory used in the model. Emission validation was essential to evaluate the accuracy.

3.2. Observation-Constrained Aromatic Emissions Calculation

Ambient aromatics concentrations were influenced by emission strength, chemical loss, deposition, transport, and mixing layer depth (Borbon et al., 2013; Saito et al., 2009). The inclusion of these processes in the emissions calculation are discussed below.

We treated Shanghai city as a single three-dimensional box with mixing layer depth (h) and area (S). Here, the value of h was 2,000 m, ensuring that the planetary boundary layer (PBL) is below the chosen height, and S was the Shanghai domain in the model. In general, the change in the aromatics concentration could be calculated via equation 1 as follows:

$$\frac{d[Aro]}{dt} = \frac{E}{S \times h} - k[O][Aro] - \frac{T}{S \times h} - \frac{D}{S \times h}, \quad (1)$$

where $[Aro]$ is the average aromatics concentration in Shanghai ($\mu\text{g m}^{-3}$); E is the emission rate ($\mu\text{g s}^{-1}$); k is the reaction rate constant of the atmospheric oxidants (O) with the aromatics ($\text{m}^3 \mu\text{g}^{-1} \text{s}^{-1}$); $[O]$ is the concentration of O, including OH radicals, ozone, and NO_3 radicals ($\mu\text{g m}^{-3}$); $k[O][Aro]$ is the chemical loss rate of aromatics ($\mu\text{g m}^{-3} \text{s}^{-1}$); T is the net transport rate out of Shanghai ($\mu\text{g s}^{-1}$), which is the gross regional export of aromatics minus regional import for the Shanghai box; and D is the dry deposition rate ($\mu\text{g s}^{-1}$).

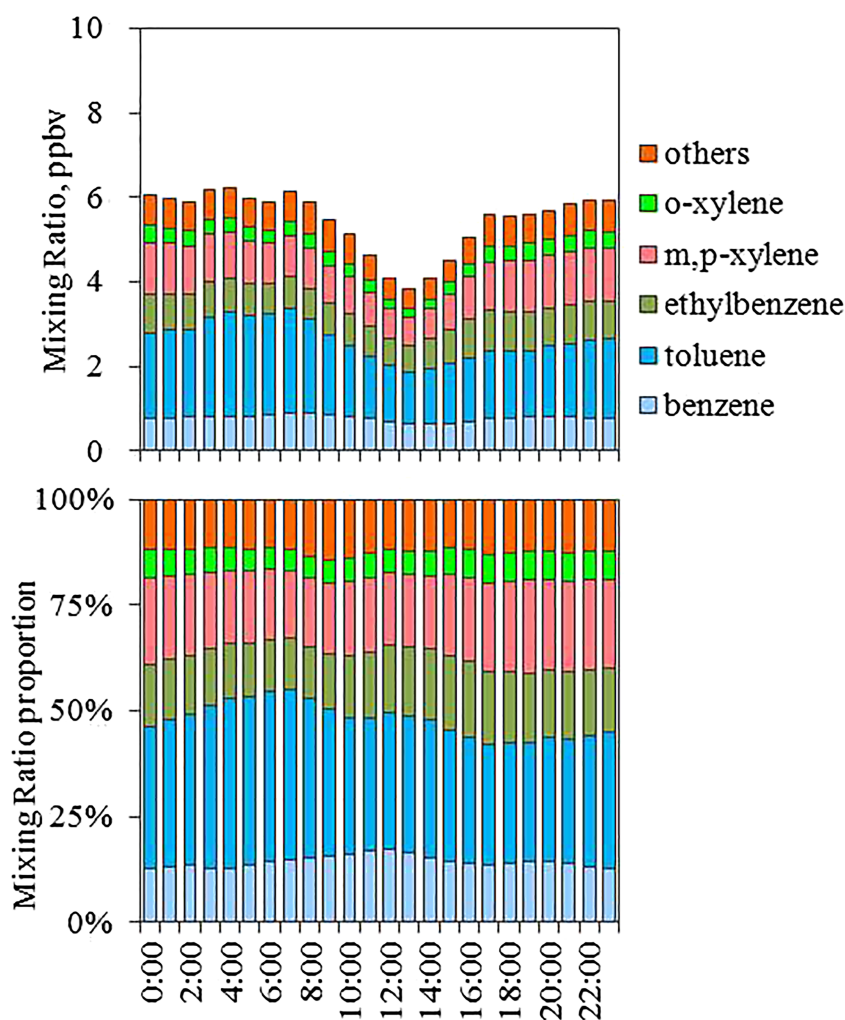


Figure 2. Diurnal variations of aromatic concentrations and speciated compositions based on the field measurements in Shanghai urban.

Equation 1 can be rearranged to solve for the aromatic emission rate (E), yielding equation 2:

$$E = S \times h \times \left(\frac{d[Aro]}{dt} + k[O][Aro] + \frac{T}{S \times h} + \frac{D}{S \times h} \right), \quad (2)$$

Hourly data were used in the budget calculation. The following sections detail the determination of each parameter in equation 2.

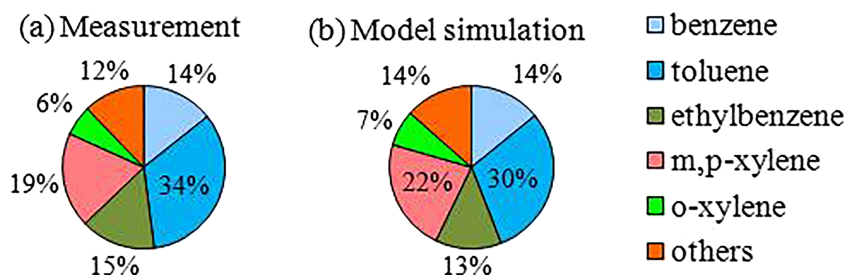


Figure 3. Speciation of aromatics (by the mixing ratio proportion) from an in situ observations and b the CMAQ model simulation.

3.2.1. Aromatic Concentrations in the Shanghai “Box”, [Aro]

Equation 2 requires horizontal and vertical spatial variations in [Aro]. However, the aromatics measurements included in this study were limited to a single surface location, at SAES. Thus, the [Aro] vertical and horizontal profiles were determined using CMAQ simulations. Monthly vertical profiles of aromatics and PBL height from model are shown in Figures S3 and S4. Aromatic concentrations in each layer varied correspondingly with the PBL height. Aromatic concentrations were highest near the surface and decreased with altitude, which became more weighted to longer-lived aromatics with height. Near the surface, nighttime concentrations are higher than daytime because of slow mixing and chemical loss at night. Above 300 m, on the other hand, nighttime concentrations are lower than daytime despite higher chemical loss in daytime because slow mixing of surface emitted aromatics to higher altitude at night. This vertical pattern of aromatics was indicative of strong surface emissions, which could be influenced by turbulent mixing, surface emissions, and atmospheric processing. Aromatic concentrations in each vertical layer could be obtained from vertical profiles and ground layer concentrations.

In terms of the horizontal variation, the aromatics concentrations at the SAES site were assumed to be representative of those in the Shanghai area because of two reasons. One was that there were no significant differences between Shanghai domain mean aromatic concentrations and aromatic concentrations in the SAES grid cell based on the model results (as shown in Figure S5; the regression slope was 1.1 with a correlation coefficient [R^2] of 0.73). More statistics results were listed in Table S3. The other was based on the measurements at 23 sites in Shanghai (Lin et al., 2019), which presented that both the concentrations and the individual compositions were similar in the averages of 23 sites and at the SAES site, with mean concentrations of 5.1 and 4.7 ppbv, respectively, although the results of the 23 sites were measured in August of 2017 and SAES results were measured in the summer (June, July, and August) of 2015, as shown in Figure S6. Hence, the measurement results at the SAES site could be used as the ground layer aromatics concentrations, and vertical concentrations were retrieved as mentioned above. Finally, [Aro] was calculated by combining the field measurements at the SAES site and the spatial variations from model with the uncertainty of 19% on average, which did not include the uncertainty of vertical patterns.

3.2.2. Chemical Loss of Aromatics, $k[O][Aro]$

Atmospheric aromatics were mainly consumed by OH radicals, ozone (O_3), and NO_3 radicals, and among them, chemical loss by OH radical was dominant (Alberto Taccone et al., 2016; Atkinson & Arey, 2003; Yuan et al., 2013). Losses of aromatics via reaction with OH, O_3 , and NO_3 are estimated and combined to evaluate the total chemical loss within the Shanghai box. Direct observations of these oxidants are lacking; assumptions regarding their concentrations are discussed below.

3.2.2.1. OH Radical Concentration

OH radical model results were presented in Figure S7, and diurnal variations in ground level OH were presented in Figure S8. Three characteristics were found. First, OH radical concentration diurnal variations exhibited maxima at noon (as shown in Figure S9), which was attributed to the dependence of OH formation on solar radiation intensity (Kulmala et al., 2005; Xue et al., 2013), and has been reported in other urban studies (Kanaya et al., 2007; Lu et al., 2012). Second, in the vertical distribution, the OH radical concentration increased slowly with the peak at a height of 1–2 km, which was approximately two times of that in the ground level (see Figure S7). To the most of our knowledge, there were few measurements of the detailed vertical distribution of OH radical concentrations in the troposphere. The model results of the OH radical concentrations increased by a factor of ~ 3 near the cloud layer (from 1 to 2 km) in the Amazon Basin (Karl et al., 2007; Kleffmann, 2005; Kuhn et al., 2007). Third, the OH radical concentration exhibited seasonal variations, with lower monthly average values in December (0.1×10^6 molecule per cubic centimeter) and higher values in August (1.9×10^6 molecule per cubic centimeter) (Figure S8). Moreover, maximum OH radical concentrations at noon increased from 0.6×10^6 molecule per cubic centimeter in December to 8.1×10^6 molecule per cubic centimeter in August (Figure S9), which was consistent with previous findings in Beijing (Lu et al., 2013; Yuan et al., 2013). Tan et al. (2019) studied the OH radical concentrations in summer of Shanghai by observation-based model, and their results were very close to our simulated OH radical concentrations. The abovementioned to some extent proved that our simulated results were reasonable. The OH radical concentrations from the CMAQ model were employed in the calculations herein because OH radical concentrations have never been measured in Shanghai. The impact of the OH concentration uncertainty on the results of these calculations is discussed in section 3.4.

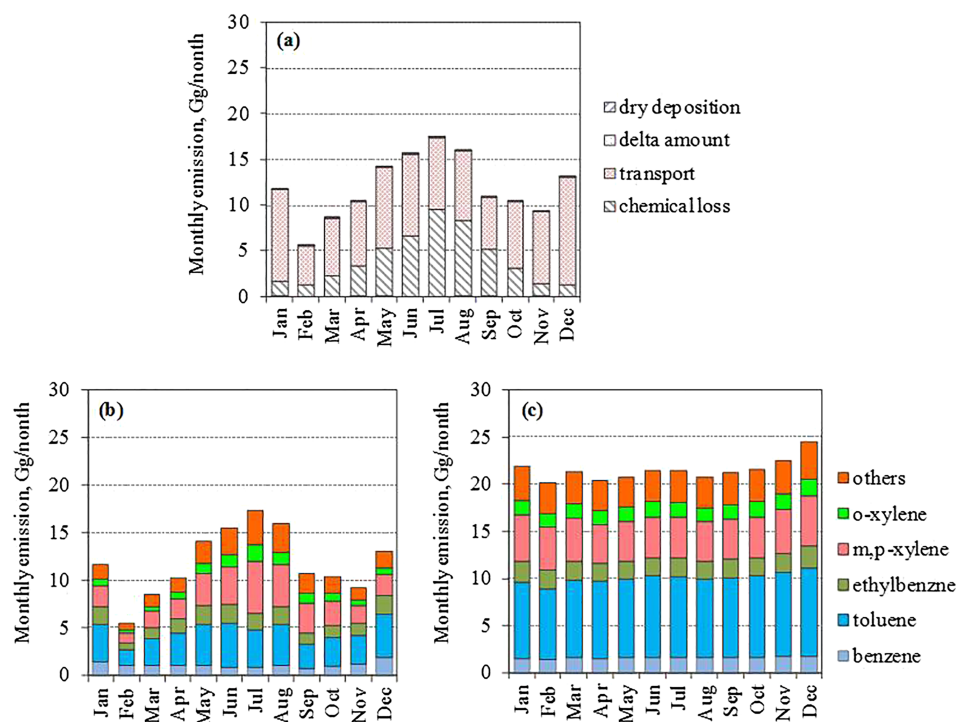


Figure 4. (a) Monthly observationally constrained aromatic emissions from this study; speciated monthly aromatic emissions (b) from this study and (c) from the MEIC aromatic emissions inventory (M. Li et al., 2019; B. Zheng et al., 2018).

3.2.2.2. NO₃ Concentration

NO₃ radical concentrations were from the model simulations. Based on the model results, the average mixing ratio of NO₃ radical was about 0.010 ± 0.006 ppbv during nighttime in the first layer (0~50 m) of the model. This value had the same order of magnitude with the measurements. Ambient NO₃ radical concentrations in the ground level were measured from 15 August to 17 October 2011 at Fudan University site (Wang et al., 2013), an urban site ~20 km northeast of SAES site, with the observed mean mixing ratio of 0.016 ± 0.009 ppbv (ranging from 0.008 to 0.095 ppbv) and a detection limit of 0.008 ppbv. In terms of the vertical distribution, the NO₃ radical mixing ratio increased with the height and the peak value (0.017 ± 0.035 ppbv) appeared in the height of 335~500 m.

3.2.2.3. O₃ Concentration

O₃ concentrations from the model simulations were directly used in the calculation. The simulated O₃ concentrations on the ground were validated by the measurements at SAES site, and the statistical results were summarized in Table S4. In general, the bias of the simulated O₃ concentrations was 3.4 ppbv on average, with the correlation coefficient of 0.74, suggesting that the simulated O₃ concentrations were acceptable. The uncertainty of this assumption was estimated below.

The total chemical loss of aromatics by OH, O₃, and NO₃ was calculated as $k[O][Aro]$, where k was the rate constant between aromatics and the oxidant and $[O]$ is the concentration of the oxidant (Atkinson, 1986; Atkinson et al., 2006; Atkinson & Arey, 2003).

As a result, the chemical loss of aromatics was 48.7 ± 12.7 Gg year⁻¹ in Shanghai in 2015, with an average of 4.1 ± 1.1 Gg month⁻¹. The chemical loss of aromatics presented large monthly variations with the peak value of 9.4 ± 3.0 Gg month⁻¹ in July and the lowest value of 1.3 ± 0.5 Gg month⁻¹ in December, as shown in Figure 4a. OH-initiated oxidation dominated aromatics consumption (99.6%, Figure S10), followed by reaction with NO₃ radicals (0.3%) and O₃ (0.1%). The dominant role of OH radicals in the chemical loss of aromatics was consistent with previous works (Atkinson, 1986; Yuan et al., 2013). Obviously, the uncertainties of chemical loss of aromatics, $k[O][Aro]$, were mainly from the uncertainties of OH radical concentrations and aromatics concentrations, which were much higher than that of the use of model results of NO₃

radical and O₃ concentrations in the calculation. The uncertainty of OH radical concentrations was assumed with a factor of 2 due to lack of measurements to validate. Accordingly, the uncertainty of the chemical loss was estimated as 26% on average, with a range of 18~38% in different months.

3.2.3. Transport Rate of Aromatics Into/Out of Shanghai, T

Aromatics transport rates out of (into) Shanghai were dependent on the surface concentrations of aromatics in Shanghai box, the surface area of Shanghai domain, and the horizontal wind speed below 2,000-m height, which were the upper boundary of the ninth layer where the maximum PBL height fell in. The transport rates out of Shanghai (T) could be calculated via equation 3.

$$T = \frac{\sum_{i=1}^m \sum_{j=1}^n ([Aro]_{i,j} \times v_{i,j})}{m \times n} \times C \times h, \quad (3)$$

where $[Aro]_{i,j}$ was the aromatics concentration in the grid in i and column j of the Shanghai box surface in horizontal direction; m was the number of surrounding grid in Shanghai domain (as outlined in section 2.3 and which number 100 herein); n was the number of vertical layers (which depended on the depth of the mixing layer); $v_{i,j}$ was the horizontal wind speed (“+” for transport out of box and “-” for transport into the box) in the i th row and j th column; C was the circumference of the Shanghai domain; and h was 2,000 m.

Based on the calculation, the transport rate of aromatics was 93.4 ± 32.7 Gg year⁻¹ in 2015, with an average of 7.8 ± 2.7 Gg month⁻¹. The transport rate of aromatics presented large monthly variations with the peak value of 11.7 ± 4.1 Gg month⁻¹ in December and the lowest value of 4.2 ± 1.4 Gg month⁻¹ in February, as shown in Figure 4a. Vertical transport out of (into) the layer of 2,000-m height was estimated by the difference (less than 6%) between the results considering those over the 2,000-m height or not, as shown in Figure S11.

3.2.4. Dry Deposition Rate, D

Dry deposition is an important air pollutant removal mechanism (Enrico et al., 2016; Zhang et al., 2002). Aromatics deposition rate (D) is calculated by multiplying the aromatics concentration by the aromatics dry deposition velocity (v_d):

$$D = v_d \times [Aro]. \quad (4)$$

v_d was calculated using the method scheme of Zhang et al. studies (L. M. Zhang et al., 2003; Zhang et al., 2002), with the average of $1e-2$ Gg month⁻¹, ranging from $6e-3$ to $3e-2$ Gg month⁻¹.

3.2.5. Delta Amount, $S \times h \times \frac{d[Aro]}{dt}$

$\frac{d[Aro]}{dt}$ (unit: $\mu\text{g m}^{-3} \text{s}^{-1}$) in each month was calculated through dividing the difference of the beginning and the end hourly concentrations by the total number of seconds in each month, as shown in Figure S12. The concentrations were from the model results but scaled by the observations at SAES site. As expected, the delta amount of aromatics in each month was close to 0.

3.3. Observation-Constrained Aromatic Emissions

According to the approach mentioned in section 3.2, a new monthly pattern of aromatic emissions constrained by the observations could be obtained. Then, we iterated the observation-constrained aromatic emissions into the model and recalculated a new emission pattern until the chemistry stable that was indicated by the OH radical concentrations. Figure 1 presented the comparison of monthly patterns of measurements, base model simulation, and final iterative observation-constrained model simulation of aromatics. As shown, by inputting the observation-constrained aromatic emissions into the model, the monthly patterns and speciation improved a lot, which were more similar to the measurements compared to the base model simulations.

3.3.1. Yearly Emissions

Estimated monthly aromatic emissions in Shanghai are presented in Figure 4a, colored by dry deposition, transport, chemical losses, and delta amount. On a yearly time scale, aromatic emissions could be divided into two parts. One was chemically consumed (yearly average proportion of 34%), which featured a

maximum contribution to total aromatic emissions of 54% in July and a minimum of 10% in December. Another part was transported out of Shanghai. Roughly 66% of the yearly average aromatic emissions were transported out of Shanghai; this value was higher (>80% in November, December, and January) in winter, suggesting that aromatic emissions in Shanghai play an important role in air pollution in downwind regions. The observation-constrained aromatic emissions herein were 142.2 ± 56.7 Gg year⁻¹ in Shanghai in 2015, which was much lower than the 2015 emission inventories (258.1 Gg year⁻¹) developed by M. Li et al. (2019) and B. Zheng et al. (2018), as shown in Figure 4c. The assumptions highlighted in the previous sections might result in some uncertainties of the total emission amount of aromatics in the present study, which were discussed below.

3.3.2. Monthly Variation

The observation-constrained aromatic emissions ranged from 5.5 ± 2.1 to 17.4 ± 7.7 Gg month⁻¹. Aromatic emissions were lowest in February (5.5 ± 2.1 Gg month⁻¹) and highest in July (17.4 ± 7.7 Gg month⁻¹), which might be due to the variations of emission activities and meteorological conditions impacting emissions (e.g., temperature). On one hand, the Spring Festival vacation occurred in February 2015 and lasted half a month, during which time, most migrant employees likely returned to their hometowns. During this time, industrial and exhaust emissions were reduced (Gu et al., 2014) compared to those of other months. On the other hand, ambient temperature also influences aromatic emissions. Evaporation processes (e.g., gasoline and solvent evaporation) depend strongly on ambient temperature (Deng & Zuo, 1999; B. Zheng et al., 2015). In addition, there might be more emission activities, like outside painting or other solvent usages, in the summer due to the favorable diffusion. Previous studies in Shanghai (Wang, Chen, et al., 2013) reported larger contributions to urban aromatics from solvent usage and vehicular emissions in summer. Thus, aromatic emissions due to evaporation would be lower during winter (February) than during summer (June, July, and August).

The monthly profile produced herein was not exhibited by emission inventories derived using bottom-up methods. Current emission inventories developed by (M. Li et al., 2019; B. Zheng et al., 2018) (Figure 4c) did not exhibit monthly variations, indicating an inability to resolve differences in monthly aromatic emissions.

3.3.3. Speciation

There were some monthly differences in the compositions of the aromatics broken down by individual species, as shown in Figure 4b and Table S5. Specifically, benzene, toluene, and ethyl benzene relative contributions to total aromatic emissions were higher in the winter than those in the summer by 19%, which were opposite to the more reactive xylenes and C9 and C10 aromatics. On a yearly basis, toluene took up 29% of the total aromatic emissions, followed by m- and p-xylene (24%), ethyl benzene (13%), benzene (9%), o-xylene (8%), and the other monocyclic aromatics contributed 17% of total aromatic emissions. The fractional composition of aromatic emissions was different from that of ambient aromatic mass concentrations. The proportions of more reactive aromatics in the total aromatic emissions are greater than the proportions of these species in the measured concentrations. For example, xylenes contribute 32% to emissions but only 27% to concentrations. The results of the more reactive species like styrene and C9–C10 aromatics (sign as “others”) were similar to that of xylenes but with larger uncertainty due to their uncertain measurements, as shown in Table S1. In contrast, the proportions of benzene, toluene, and ethyl benzene are lower in emissions (52%) than in concentrations (59%). One very possible and important reason was the enhanced removal of the more reactive aromatics prior to arrival at the SAES receptor measurement site.

The species distribution differed from that in MEIC emission inventory developed by M. Li et al. (2019) and B. Zheng et al. (2018) (Figure 4c), in which toluene and m- and p-xylene mass fractions were 39% and 21%, respectively, and ethyl benzene, benzene, and o-xylene contributed 9%, 8%, and 7%, respectively. It suggested that more insight into VOCs source profiles was critical to the development of accurate species emission inventories.

3.4. Uncertainty Analysis

In this study, we assumed the response relationship of the emissions input and aromatic concentrations on a monthly basis was reasonable in CMAQ simulations. Specifically, the assumption implies the following.

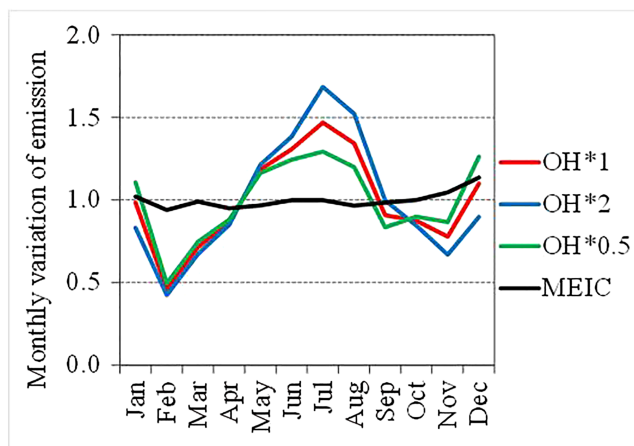


Figure 5. Sensitivity of monthly patterns of aromatic emissions under different OH radical concentrations, scaled by the monthly average emission. OH*1, model-simulated concentrations of OH radical; OH*2, model-simulated concentrations by a factor of 2; OH*0.5, model-simulated concentrations by a factor of 0.5; MEIC: monthly patterns of MEIC emissions inventory.

3.4.1. Uncertainty of [Aro]

The first assumption was that the spatial patterns of aromatics, including the horizontal and vertical patterns, were reasonable, and the observed aromatics in SAES site were used to scale the model results to obtain the spatial concentrations of aromatics in domain O3. In terms of the horizontal variation, the aromatic concentrations at the SAES site were assumed to be representative of the Shanghai area, which were discussed in section 3.2.1. The uncertainty of the vertical distribution assumption could not be evaluated in the present study due to a lack of observation data.

Thus, the uncertainty of [Aro] could be estimated by the uncertainty of aromatic measurements (listed in Table S1) and the uncertainty of horizontal patterns (~10%) mentioned in section 3.2.1. As a result, the uncertainty of [Aro] was estimated as about 19%.

3.4.2. Uncertainty of [O]

The second assumption was that the simulated concentrations of OH radical, NO₃ radical, and O₃ were reasonable. Considering the oxidation of aromatics by NO₃ radical and O₃ was negligible (~0.4%), the uncertainty of this assumption was mainly from the simulated OH radical concentrations. The simulated OH radical concentrations (as shown in Figures

S7–S9) were hard to validate due to lack of measurements in Shanghai. While our simulated OH radical concentrations were comparable with the measurements in other cities of eastern China, like Beijing (Lu et al., 2013; Yuan et al., 2013). Tan et al. (2019) studied the OH radical concentrations in summer of Shanghai by observation-based model, and their results were very close to our simulated OH radical concentrations. Different OH radical concentration levels (i.e., model results multiplied by factors of 1, 2, and 0.5; in other words, with an uncertainty of 100%) were tested. The sensitivity analysis gave similar monthly aromatic emissions patterns, which were very different from that of MEIC emission inventory, as shown in Figure 5.

3.4.3. Uncertainty of the Meteorology

The third assumption was that the atmospheric physics of the model was reasonable, and the meteorological conditions simulated in the model, including the barometric pressure, temperature, and wind speeds, were used directly in the present calculation. The WRF performance in the ground level was validated using the measurements at Pudong International Airport in Shanghai. The ranges of biases, summarized in Table S2, mostly met the model performance criteria recommended by Emery et al. (2001) for retrospective regional-scale model applications, which are $\leq \pm 0.5$ K, $\leq \pm 1.0$ g/kg, $\leq \pm 0.5$ m s⁻¹, and $\leq \pm 10^\circ$, respectively, suggesting that the meteorology simulations in this study were acceptable. The evaluation of WRF performance ensured that there was no significant bias in the meteorological fields used in the coupled model.

Due to a lack of enough vertical measurements, the uncertainty of simulated meteorological conditions was hard to be estimated even though we have ground measurements. Zhao and Wang (2009) investigated the impact of meteorology on the model results by comparing the simulated tropospheric NO₂ columns using either WRF or MM5 assimilated meteorological fields, and the monthly mean of absolute error was mostly <30% with an average of 11%. As there was no similar study of aromatics, we applied the above results (the upper uncertainty, 30%) as the uncertainty of simulated meteorology in the present study considering the similar lifetime of NO₂ and aromatics (within one order of magnitude).

In summary, the uncertainties were estimated considering the assumptions and measurements biases as much as possible, including the uncertainty of observations aromatics (15.8%), the representativeness of SAES site (~10%, estimated by the difference of SAES site measurement and the spatial [23 sites] measurements in Shanghai), the underestimation of transport out of the 2,000-m height (6%) as mentioned in section 3.2.3, the simulation of the meteorology (30%; Zhao & Wang, 2009), and the simulated OH radical concentrations (assuming a uncertainty of 100%). On average, the uncertainty was estimated as 36%, ranging from 32% to 43% in different months, as shown in Figure 6.

The present study provided one new approach to constrain the emissions inventory by observations combining with 3-D model, and the results were dependent on the model performance with the assumption that the

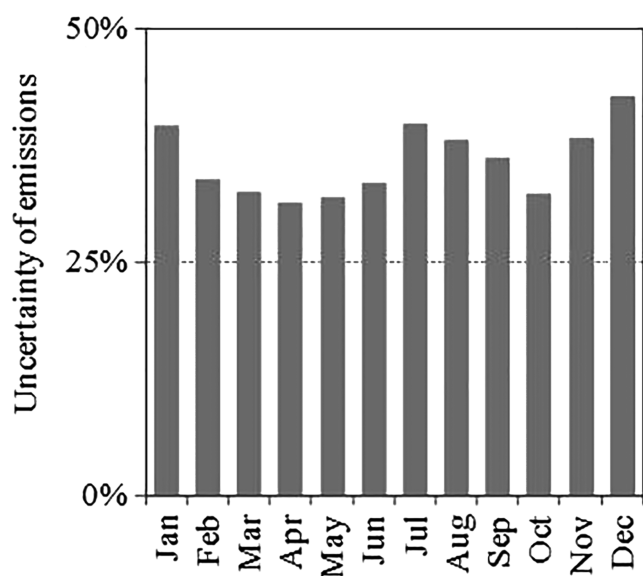


Figure 6. The uncertainty of monthly emissions considering the bias of observations aromatics (15.8%), the representativeness of SAES site (~10%, estimated by the difference of SAES site measurement and the spatial [23 sites] measurements in Shanghai), the underestimation of transport out of the 2,000-m height (6%), the simulated meteorology (30%; Zhao & Wang, 2009), and the simulated OH radical concentrations (assuming an uncertainty of 100%).

response relationship of the emissions input and the simulated aromatic concentrations on a monthly basis was reasonable in CMAQ simulations. In using this approach, the uncertainty of the results was estimated with all accessible measurements including chemicals and meteorology in the present study.

The level of uncertainties included in this study are no more than a typical modeling study. We believe integrating the observations with modeling as we did in this study will be used more and more in air quality studies, and the associated uncertainties need to be clearly quantified as we did in this study. Further studies and measurements are needed to assess the validity of these assumptions and their impacts on the estimates of aromatics emissions.

4. Conclusions

Aromatics are critically important precursors of ozone and SOA formation in the urban troposphere. However, aromatic emission inventories based on bottom-up method featured large uncertainties. Significant differences in monthly aromatic trends have been found between measurements and model results in Shanghai. To address this shortcoming, this study used observationally constrained aromatic emissions to validate the bottom-up emission inventory. Herein, aromatic emissions constrained by observations were calculated using CMAQ model results and 1-year continuous measurements of aromatics at SAES site of Shanghai in 2015. The resulting aromatic emissions in Shanghai was $142.2 \pm 56.7 \text{ Gg year}^{-1}$, being much lower than that ($258.1 \text{ Gg year}^{-1}$) of

MEIC emission inventory. In particular, the observation-constrained aromatic emissions exhibited monthly variations. The largest value ($17.4 \pm 7.7 \text{ Gg month}^{-1}$) was in July, being ~3.2 times of that ($5.5 \pm 2.1 \text{ Gg month}^{-1}$) in February and ~1.4 times of the monthly average ($11.9 \pm 4.7 \text{ Gg month}^{-1}$). Toluene, xylenes, and ethyl benzene dominated the total aromatic emissions (contributing 66% on average) but showed considerable monthly variations.

In addition to the large difference of temporal variation, the observation-constrained emissions showed different speciation from the bottom-up emission inventory. In the MEIC emission inventory, toluene and m- and p-xylene were the top two species, with proportions of 39% and 21% on annual average, respectively, followed by ethylbenzene (9%), benzene (8%), o-xylene (7%), and C9~C10 aromatics (16%). In comparison, toluene and m- and p-xylene contributed 29% and 24% of the emissions obtained in this study, followed by ethylbenzene (13%), benzene (9%), and o-xylene (8%). Therefore, the relative contribution of toluene emissions was overestimated the most in the emission inventory, while that of C8 aromatics was underestimated the most in the emission inventory.

Aromatics have been reported as the most important anthropogenic VOC precursors of ozone and SOA in most of eastern China (Gao et al., 2019; Wang, Chen, et al., 2013). With stronger solar radiation in summer, aromatic photochemistry was more active to enhance the formation of ozone and SOA than expected due to more emissions in summer. Further work was essential to assess the impact of the changes of emissions on ozone and SOA estimation in Shanghai and other cities.

Acknowledgments

This work was supported by the National Key R&D Program of China (2018YFC0213801), the National Natural Science Foundation of China (21607104), the Shanghai Science and Technology Commission of the Shanghai Municipality (18QA1403600). Y. Wang was supported by the U.S. NSF Atmospheric Chemistry Program. The data in the present study can be found at <https://doi.org/10.17632/fh5pbn5s9.1> (Wang, 20202020).

References

- Alberto Taccone, R., Moreno, A., Colmenar, I., Salgado, S., Pilar Martin, M., & Cabanas, B. (2016). Kinetic study of the OH, NO₃ radicals and Cl atom initiated atmospheric photo-oxidation of iso-propenyl methyl ether. *Atmospheric Environment*, *127*, 80–89. <https://doi.org/10.1016/j.atmosenv.2015.12.033>
- Atkinson, R. (1986). Kinetics and mechanisms of the gas-phase reactions of the hydroxyl radical with organic compounds under atmospheric conditions. *Chemical Reviews*, *86*(1), 69–201. <https://doi.org/10.1021/cr00071a004>
- Atkinson, R. (2000). Atmospheric chemistry of VOCs and NO_x. *Atmospheric Environment*, *34*(12–14), 2063–2101. [https://doi.org/10.1016/s1352-2310\(99\)00460-4](https://doi.org/10.1016/s1352-2310(99)00460-4)
- Atkinson, R., & Arey, J. (2003). Atmospheric degradation of volatile organic compounds. *Chemical Reviews*, *103*(12), 4605–4638. <https://doi.org/10.1021/cr0206420>

- Atkinson, R., Baulch, D. L., Cox, R. A., Crowley, J. N., Hampson, R. F., Hynes, R. G., et al. (2006). Evaluated kinetic and photochemical data for atmospheric chemistry: Volume II—Gas phase reactions of organic species. *Atmospheric Chemistry and Physics*, 6, 3625–4055.
- Barletta, B., Meinardi, S., Rowland, F. S., Chan, C. Y., Wang, X. M., Zou, S. C., et al. (2005). Volatile organic compounds in 43 Chinese cities. *Atmospheric Environment*, 39(32), 5979–5990. <https://doi.org/10.1016/j.atmosenv.2005.06.029>
- Borbon, A., Gilman, J. B., Kuster, W. C., Grand, N., Chevaillier, S., Colomb, A., et al. (2013). Emission ratios of anthropogenic volatile organic compounds in northern mid-latitude megacities: Observations versus emission inventories in Los Angeles and Paris. *Journal of Geophysical Research: Atmospheres*, 118(4), 2041–2057. <https://doi.org/10.1002/jgrd.50059>
- Cabrera-Perez, D., Taraborrelli, D., Sander, R., & Pozzer, A. (2016). Global atmospheric budget of simple monocyclic aromatic compounds. *Atmospheric Chemistry and Physics*, 16(11), 6931–6947. <https://doi.org/10.5194/acp-16-6931-2016>
- Ceron-Breton, J. G., Ceron-Breton, R. M., Kahl, J., Ramirez-Lara, E., Guarnaccia, C., Aguilar-Ucan, C., et al. (2015). Diurnal and seasonal variation of BTEX in the air of Monterrey, Mexico: Preliminary study of sources and photochemical ozone pollution. *Air Quality Atmosphere and Health*, 8(5), 469–482. <https://doi.org/10.1007/s11869-014-0296-1>
- Chen, S. P., Liu, T. H., Chen, T. F., Yang, C. F. O., Wang, J. L., & Chang, J. S. (2010). Diagnostic Modeling of PAMS VOC observation. *Environmental Science & Technology*, 44(12), 4635–4644. <https://doi.org/10.1021/es903361r>
- de Gouw, J. A. (2005). Budget of organic carbon in a polluted atmosphere: Results from the New England air quality study in 2002. *Journal of Geophysical Research*, 110(D16). <https://doi.org/10.1029/2004jd005623>
- Deng, Y. W., & Zuo, Y. G. (1999). Factors affecting the levels of hydrogen peroxide in rainwater. *Atmospheric Environment*, 33(9), 1469–1478. [https://doi.org/10.1016/s1352-2310\(98\)00239-8](https://doi.org/10.1016/s1352-2310(98)00239-8)
- Ding, X., Wang, X.-M., Gao, B., Fu, X.-X., He, Q.-F., Zhao, X.-Y., et al. (2012). Tracer-based estimation of secondary organic carbon in the Pearl River Delta, South China. *Journal of Geophysical Research*, 117. <https://doi.org/10.1029/2011jd016596>
- Emery, C., Tai, E., & Yarwood, G. (2001). Enhanced meteorological modeling and performance evaluation for two Texas ozone episodes [J]. Prepared for the Texas natural resource conservation commission, by ENVIRON International Corporation.
- Enrico, M., Le Roux, G., Maruschak, N., Heimburger, L. E., Claustres, A., Fu, X. W., et al. (2016). Atmospheric mercury transfer to peat bogs dominated by gaseous elemental mercury dry deposition. *Environmental Science & Technology*, 50(5), 2405–2412. <https://doi.org/10.1021/acs.est.5b06058>
- Fu, T. M., Jacob, D. J., Palmer, P. I., Chance, K., Wang, Y. X. X., Barletta, B., et al. (2007). Space-based formaldehyde measurements as constraints on volatile organic compound emissions in East and South Asia and implications for ozone. *Journal of Geophysical Research: Atmospheres*, 112, D06312. <https://doi.org/10.1029/2006jd007853>
- Gao, Y., Wang, H., Zhang, X., Jing, S., Peng, Y., Qiao, L., et al. (2019). Estimating secondary organic aerosol production from toluene photochemistry in a megacity of China. *Environmental Science & Technology*, 53(15), 8664–8671. <https://doi.org/10.1021/acs.est.9b00651>
- Gu, D., Wang, Y., Smeltzer, C., & Boersma, K. F. (2014). Anthropogenic emissions of NO_x over China: Reconciling the difference of inverse modeling results using GOME-2 and OMI measurements. *Journal of Geophysical Research: Atmospheres*, 119, 7732–7740. <https://doi.org/10.1002/2014jd021644>
- Guo, S., Hu, M., Shang, D., Guo, Q., & Hu, W. (2014). Research on secondary organic aerosols basing on field measurement. *Acta Chimica Sinica*, 72(2), 145. <https://doi.org/10.6023/a13111169>
- Hsu, Y. K., VanCuren, T., Park, S., Jakober, C., Herner, J., FitzGibbon, M., et al. (2010). Methane emissions inventory verification in southern California. *Atmospheric Environment*, 44(1), 1–7. <https://doi.org/10.1016/j.atmosenv.2009.10.002>
- Kanakidou, M., Seinfeld, J. H., Pandis, S. N., Barnes, I., Dentener, F. J., Facchini, M. C., et al. (2005). Organic aerosol and global climate modelling: A review. *Atmospheric Chemistry and Physics*, 5, 1053–1123.
- Kanaya, Y., Cao, R., Akimoto, H., Fukuda, M., Komazaki, Y., Yokouchi, Y., et al. (2007). Urban photochemistry in central Tokyo: 1. Observed and modeled OH and HO₂ radical concentrations during the winter and summer of 2004. *Journal of Geophysical Research*, 112. <https://doi.org/10.1029/2007jd008670>
- Kansal, A. (2009). Sources and reactivity of NMHCs and VOCs in the atmosphere: A review. *Journal of Hazardous Materials*, 166(1), 17–26. <https://doi.org/10.1016/j.jhazmat.2008.11.048>
- Karl, T., Guenther, A., Yokelson, R. J., Greenberg, J., Potosnak, M., Blake, D. R., & Artaxo, P. (2007). The tropical forest and fire emissions experiment: Emission, chemistry, and transport of biogenic volatile organic compounds in the lower atmosphere over Amazonia. *Journal of Geophysical Research*, 112. <https://doi.org/10.1029/2007jd008539>
- Kleffmann, J. (2005). Daytime formation of nitrous acid: A major source of OH radicals in a forest. *Geophysical Research Letters*, 32(5). <https://doi.org/10.1029/2005gl022524>
- Kuhn, U., Andreae, M. O., Ammann, C., Araújo, A. C., Brancaleoni, E., Ciccioli, P., et al. (2007). Isoprene and monoterpene fluxes from Central Amazonian rainforest inferred from tower-based and airborne measurements, and implications on the atmospheric chemistry and the local carbon budget. *Atmospheric Chemistry and Physics*, 7(11), 2855–2879. <https://doi.org/10.5194/acp-7-2855-2007>
- Kulmala, M., Petaja, T., Monkkonen, P., Koponen, I. K., Dal Maso, M., Aalto, P. P., et al. (2005). On the growth of nucleation mode particles: Source rates of condensable vapor in polluted and clean environments. *Atmospheric Chemistry and Physics*, 5, 409–416. <https://doi.org/10.5194/acp-5-409-2005>
- Kumar, A., Singh, D., Kumar, K., Singh, B. B., & Jain, V. K. (2018). Distribution of VOCs in urban and rural atmospheres of subtropical India: Temporal variation, source attribution, ratios, OFP and risk assessment. *Science of the Total Environment*, 613–614, 492–501. <https://doi.org/10.1016/j.scitotenv.2017.09.096>
- Lee, S. C., Chiu, M. Y., Ho, K. F., Zou, S. C., & Wang, X. M. (2002). Volatile organic compounds (VOCs) in urban atmosphere of Hong Kong. *Chemosphere*, 48(3), 375–382. [https://doi.org/10.1016/s0045-6535\(02\)00040-1](https://doi.org/10.1016/s0045-6535(02)00040-1)
- Li, L., An, J. Y., Shi, Y. Y., Zhou, M., Yan, R. S., Huang, C., et al. (2016). Source apportionment of surface ozone in the Yangtze River Delta, China in the summer of 2013. *Atmospheric Environment*, 144, 194–207. <https://doi.org/10.1016/j.atmosenv.2016.08.076>
- Li, L., Chen, C. H., Huang, C., Huang, H. Y., Zhang, G. F., Wang, Y. J., et al. (2012). Process analysis of regional ozone formation over the Yangtze River Delta, China using the community multi-scale air quality modeling system. *Atmospheric Chemistry and Physics*, 12(22), 10,971–10,987. <https://doi.org/10.5194/acp-12-10971-2012>
- Li, M., Zhang, Q., Streets, D. G., He, K. B., Cheng, Y. F., Emmons, L. K., et al. (2014). Mapping Asian anthropogenic emissions of non-methane volatile organic compounds to multiple chemical mechanisms. *Atmospheric Chemistry and Physics*, 14(11), 5617–5638. <https://doi.org/10.5194/acp-14-5617-2014>
- Li, M., Zhang, Q., Zheng, B., Tong, D., Lei, Y., Liu, F., et al. (2019). Persistent growth of anthropogenic non-methane volatile organic compound (NMVOC) emissions in China during 1990–2017: Drivers, speciation and ozone formation potential. *Atmospheric Chemistry and Physics*, 19(13), 8897–8913. <https://doi.org/10.5194/acp-19-8897-2019>

- Lin, Y., Duan, Y., Gao, Z., Lin, C., Zhou, S., Song, Z., et al. (2019). Typical ozone pollution process and source identification in Shanghai based on VOCs intense measurement, *Acta Scientiae Circumstantiae*, 39(1), 126–133. <https://doi.org/10.13671/j.hjkxxb.2018.0242>.
- Liu, Y., Li, L., An, J., Huang, L., Yan, R., Huang, C., et al. (2018). Estimation of biogenic VOC emissions and its impact on ozone formation over the Yangtze River Delta region, China. *Atmospheric Environment*, 186, 113–128. <https://doi.org/10.1016/j.atmosenv.2018.05.027>
- Liu, Y., Wang, H., Jing, S., Gao, Y., Peng, Y., Lou, S., et al. (2019). Characteristics and sources of volatile organic compounds (VOCs) in Shanghai during summer: Implications of regional transport. *Atmospheric Environment*, 215, 116,902. <https://doi.org/10.1016/j.atmosenv.2019.116902>
- Liu, Z., Wang, Y., Gu, D., Zhao, C., Huey, L. G., Stickel, R., et al. (2012). Summertime photochemistry during CAREBeijing-2007: RO_x budgets and O₃ formation. *Atmospheric Chemistry and Physics*, 12(16), 7737–7752. <https://doi.org/10.5194/acp-12-7737-2012>
- Liu, Z., Wang, Y., Vrekoussis, M., Richter, A., Wittrock, F., Burrows, J. P., et al. (2012). Exploring the missing source of glyoxal (CHOCHO) over China. *Geophysical Research Letters*, 39. <https://doi.org/10.1029/2012gl051645>
- Lu, K. D., Hofzumahaus, A., Holland, F., Bohn, B., Brauers, T., Fuchs, H., et al. (2013). Missing OH source in a suburban environment near Beijing: Observed and modelled OH and HO₂ concentrations in summer 2006. *Atmospheric Chemistry and Physics*, 13(2), 1057–1080. <https://doi.org/10.5194/acp-13-1057-2013>
- Lu, K. D., Rohrer, F., Holland, F., Fuchs, H., Bohn, B., Brauers, T., et al. (2012). Observation and modelling of OH and HO₂ concentrations in the Pearl River Delta 2006: A missing OH source in a VOC rich atmosphere. *Atmospheric Chemistry and Physics*, 12(3), 1541–1569. <https://doi.org/10.5194/acp-12-1541-2012>
- Ran, L., Zhao, C. S., Geng, F. H., Tie, X. X., Tang, X., Peng, L., et al. (2009). Ozone photochemical production in urban Shanghai, China: Analysis based on ground level observations. *Journal of Geophysical Research*, 114. <https://doi.org/10.1029/2008jd010752>
- Saito, S., Nagao, I., & Kanzawa, H. (2009). Characteristics of ambient C₂-C₁₁ non-methane hydrocarbons in metropolitan Nagoya, Japan. *Atmospheric Environment*, 43(29), 4384–4395. <https://doi.org/10.1016/j.atmosenv.2009.04.031>
- Seinfeld, J. H., & Pandis, S. N. (2012). *Atmospheric chemistry and physics: From air pollution to climate change*. New York: John Wiley & Sons.
- Shao, M., Huang, D., Gu, D., Lu, S., Chang, C., & Wang, J. (2011). Estimate of anthropogenic halocarbon emission based on measured ratio relative to CO in the Pearl River Delta region, China. *Atmospheric Chemistry and Physics*, 11(10), 5011–5025. <https://doi.org/10.5194/acp-11-5011-2011>
- Shao, P., An, J., Xin, J., Wu, F., Wang, J., Ji, D., & Wang, Y. (2016). Source apportionment of VOCs and the contribution to photochemical ozone formation during summer in the typical industrial area in the Yangtze River Delta, China. *Atmospheric Research*, 176, 64–74. <https://doi.org/10.1016/j.atmosres.2016.02.015>
- Tan, Z., Lu, K., Jiang, M., Su, R., Wang, H., Lou, S., et al. (2019). Daytime atmospheric oxidation capacity in four Chinese megacities during the photochemically polluted season: A case study based on box model simulation. *Atmospheric Chemistry and Physics*, 19(6), 3493–3513. <https://doi.org/10.5194/acp-19-3493-2019>
- Wang, H. L., Chen, C. H., Wang, Q., Huang, C., Su, L. Y., Huang, H. Y., et al. (2013). Chemical loss of volatile organic compounds and its impact on the source analysis through a two-year continuous measurement. *Atmospheric Environment*, 80, 488–498. <https://doi.org/10.1016/j.atmosenv.2013.08.040>
- Wang, H. L., Qiao, L. P., Lou, S. R., Zhou, M., Ding, A. J., Huang, H. Y., et al. (2016). Chemical composition of PM_{2.5} and meteorological impact among three years in urban Shanghai, China. *Journal of Cleaner Production*, 112, 1302–1311. <https://doi.org/10.1016/j.jclepro.2015.04.099>
- Wang, H. (2020). “Observation constrained aromatic emissions in Shanghai-2019JD031815 DATA”, Mendeley Data, v1
- Wang, M., Shao, M., Chen, W., Yuan, B., Lu, S., Zhang, Q., et al. (2014). A temporally and spatially resolved validation of emission inventories by measurements of ambient volatile organic compounds in Beijing, China. *Atmospheric Chemistry and Physics*, 14(12), 5871–5891. <https://doi.org/10.5194/acp-14-5871-2014>
- Wang, S., Zhou, R., Zhao, H., Wang, Z., Chen, L., & Zhou, B. (2013). Long-term observation of atmospheric nitrous acid (HONO) and its implication to local NO₂ levels in Shanghai, China. *Atmospheric Environment*, 77, 718–724. <https://doi.org/10.1016/j.atmosenv.2013.05.071>
- Wang, Y. P., Teng, C. T., Vieira, A. H., Gorenstein, C., & Andrade, L. H. (2014). Source profiles and chemical reactivity of volatile organic compounds from solvent use in Shanghai, China. *Aerosol and Air Quality Research*, 14(1), 301–310. <https://doi.org/10.4209/aaqr.2013.03.0064>
- Xue, L. K., Wang, T., Guo, H., Blake, D. R., Tang, J., Zhang, X. C., et al. (2013). Sources and photochemistry of volatile organic compounds in the remote atmosphere of western China: Results from the Mt. Waliguan Observatory. *Atmospheric Chemistry and Physics*, 13(17), 8551–8567. <https://doi.org/10.5194/acp-13-8551-2013>
- Yuan, B., Hu, W. W., Shao, M., Wang, M., Chen, W. T., Lu, S. H., et al. (2013). VOC emissions, evolutions and contributions to SOA formation at a receptor site in eastern China. *Atmospheric Chemistry and Physics*, 13(17), 8815–8832. <https://doi.org/10.5194/acp-13-8815-2013>
- Zhang, L. M., Brook, J. R., & Vet, R. (2002). On ozone dry deposition-With emphasis on non-stomatal uptake and wet canopies. *Atmospheric Environment*, 36(30), 4787–4799. [https://doi.org/10.1016/s1352-2310\(02\)00567-8](https://doi.org/10.1016/s1352-2310(02)00567-8)
- Zhang, L. M., Brook, J. R., & Vet, R. (2003). Evaluation of a non-stomatal resistance parameterization for SO₂ dry deposition. *Atmospheric Environment*, 37(21), 2941–2947. [https://doi.org/10.1016/s1352-2310\(03\)00268-1](https://doi.org/10.1016/s1352-2310(03)00268-1)
- Zhang, L. M., Moran, M. D., Makar, P. A., Brook, J. R., & Gong, S. L. (2002). Modelling gaseous dry deposition in AURAMS: A unified regional air-quality modelling system. *Atmospheric Environment*, 36(3), 537–560. [https://doi.org/10.1016/s1352-2310\(01\)00447-2](https://doi.org/10.1016/s1352-2310(01)00447-2)
- Zhang, R., Wang, Y., He, Q., Chen, L., Zhang, Y., Qu, H., et al. (2017). Enhanced trans-Himalaya pollution transport to the Tibetan Plateau by cut-off low systems. *Atmospheric Chemistry and Physics*, 17(4), 3083–3095. <https://doi.org/10.5194/acp-17-3083-2017>
- Zhao, C., & Wang, Y. (2009). Assimilated inversion of NO_x emissions over East Asia using OMI NO₂ column measurements. *Geophysical Research Letters*, 36(6). <https://doi.org/10.1029/2008gl037123>
- Zheng, B., Tong, D., Li, M., Liu, F., Hong, C., Geng, G., et al. (2018). Trends in China’s anthropogenic emissions since 2010 as the consequence of clean air actions. *Atmospheric Chemistry and Physics*, 18(19), 14,095–14,111. <https://doi.org/10.5194/acp-18-14095-2018>
- Zheng, B., Zhang, Q., Zhang, Y., He, K. B., Wang, K., Zheng, G. J., et al. (2015). Heterogeneous chemistry: A mechanism missing in current models to explain secondary inorganic aerosol formation during the January 2013 haze episode in North China. *Atmospheric Chemistry and Physics*, 15(4), 2031–2049. <https://doi.org/10.5194/acp-15-2031-2015>